

HST OBSERVATIONS OF BLUE STRAGGLER STARS IN THE CORE OF THE GLOBULAR CLUSTER M3

F.R. Ferraro¹, B. Paltrinieri¹, F. Fusi Pecci^{1,2}, C. Cacciari^{1,3}, B. Dorman^{4,5}, R.T. Rood⁵, R. Buonanno⁶,
C.E. Corsi⁶, D. Burgarella⁷, M. Laget⁷

¹ Osservatorio Astronomico di Bologna, Via Zamboni 33, I-40126 Bologna, ITALY

² Stazione Astronomica di Cagliari, 09012 Capoterra, ITALY

³ Space Telescope Science Institute, Baltimore, USA

⁴ Goddard Space Flight Center, NASA Greenbelt, USA

⁵ University of Virginia, Charlottesville, USA

⁶ Osservatorio Astronomico di Roma, Roma, ITALY

⁷ Laboratoire d'Astronomie Spatiale, CNRS Marseille, FRANCE

Abstract. The core of the Galactic Globular Cluster M3 (NGC 5272) has been observed with the WFPC2 through the filters *F255W*, *F336W*, *F555W*, and *F814W*. Using these observations along with a thorough reanalysis of earlier catalogs, we have produced a catalog of blue straggler stars (BSS) spanning the cluster. Earlier studies and the fainter part of our sample suffer severe selection biases. Our analysis is based on a more reliable *bright global sample* of 122 BSS. We confirm earlier suggestions that the radial BSS distribution in M3 is bimodal. It is strongly peaked in the center, has a clear dip 100–200'' from the center, and rises again at larger radii. The observed distribution agrees with the dynamical model of Sigurdsson et al. (1994) which takes into account both star collisions and merging of primordial binaries for the origin of BSS. The observed luminosity functions of BSS in the inner and outer parts of the cluster are different. Interpreting these using the models of Bailyn & Pinsonneault (1995), we suggest that the BSS in the inner cluster are formed by stellar collisions and those in the outer cluster from merging primordial binaries.

Key words: Clusters: globular - Stars: Population II - Stars: Blue Stragglers

1. Introduction

With the advent of high-resolution, highly accurate imaging facilities, there has been a growing interest in the systematic search and study of Blue Straggler Stars (BSS)

Send offprint requests to: F.R. Ferraro, e-mail ferraro@astbo3.bo.astro.it

in Galactic Globular Clusters (GGCs). BSS were first detected in the GGC M3 by Sandage (1953) and by 1995 there were more than 700 BSS candidates identified in about 35 GGCs (see the review of Bailyn 1995 and the catalogs of Ferraro et al. 1993, 1995, Sarajedini 1993). The BSS sample is increasing rapidly as more GGC cores are adequately surveyed with the *Hubble Space Telescope* (*HST*).

Even with the dramatic increase in the known BSS population, the most interesting cluster population of BSS remains that in M3. This is the only bright cluster where the radial distribution of BSS has been studied extensively. In particular, Ferraro et al. (1993, hereafter F93) found a bimodal radial distribution of the BSS candidates. This could arise if there were different BSS formation mechanisms at work in regions of different stellar density. For example, the external areas would contain mostly BSS that were formed in primordial binary mergers, whereas the core would contain mostly BSS formed via collisions (see Bailyn & Pinsonneault 1995, hereafter BP95, and Bailyn 1995, for a general discussion and references). Alternatively, one could imagine that, though formed via the same mechanism, the BSS have been subject to radial mass segregation or suffered different disruption/survival histories.

This situation is apparently unique to M3; no other cluster has been found to show this bimodal distribution of BSS. In addition M3 serves as an archetype for several astrophysical problems—e.g., its “horizontal” horizontal branch gave the name to the sequence. It has been well studied both photometrically and spectroscopically. Because of these factors we have selected M3 as a primary target for a long term project investigating the global populations of globular clusters, in spite of the fact that it is not the nearest cluster in the sky.

During the last decade we have secured in M3 one of the *widest and most complete* samples of stars ever observed in a globular cluster using different techniques (photographic plates: Buonanno et al. 1986, 1994 [PH94], and CCD-arrays: Ferraro et al. 1997 [CCD97]), covering most of the cluster area (from $20''$ up to $7'$ from the cluster center). To achieve the ultimate in sample size and completeness and to check for radial variations in the cluster population, we obtained high-resolution *HST* observations during Cycle 4 (GO 5496 P.I. F. Fusi Pecci) aimed at completing the survey in the inner regions. The project as a whole aimed at testing the accuracy and validity of the assumptions and physical inputs that are the foundation of the current stellar evolution theoretical models.

This paper is the first of a series reporting on the results obtained from the global Colour-Magnitude Diagrams (CMDs) and Luminosity Functions (LFs). Here we present results on BSS candidates in the cluster core and discuss the distribution of BSS across the cluster.

2. Observations, data reduction

A more detailed descriptions of observations and reductions will be given elsewhere (Fusi Pecci et al. 1997). We outline here the important points.

The *HST* frames were obtained on 1995, April 25 (GO 5496) with the WFPC2 coupled with the filters $F255W$ (m_{255}), $F336W$ (U), $F555W$ (V), and $F814W$ (I). The PC was roughly centered on the cluster center, while the WF cameras partially overlapped outer regions previously observed from the ground (see Figure 1). While complete reductions have already been carried out for most available frames, here we make use only of the $F255W$, $F336W$ and $F555W$ observations for all four chips (PC, WF2, WF3, WF4) and $F814W$ data for the PC. The list of the frames and the exposure times per frame are reported in Table 1.

Each WFPC2 frame was processed through the standard HST-WFPC2 pipeline for bias subtraction, dark correction, and flat-fielding. Then, all the long exposure images were registered using MIDAS, obtaining a median frame where the cosmic rays have been removed. We used the median frame in order to search for all the individual star components present in each field following the standard procedure implemented in ROMAFOT (Buonanno et al. 1993), a package specifically developed for high precision photometry in crowded fields. The PSF fitting photometry was performed on each individual frame separately, and an averaged instrumental magnitude was computed for each star. The instrumental magnitudes (m_{instr}) were finally transformed to the Johnson system (for V , I , U , respectively) using formula 8 and Table 7 from Holtzmann et al. (1995), and in the STMAG system using Table 9 for the $F255W$ filter.

Figure 2 shows the CMD (m_{255} , $m_{255} - U$) for more than 18,000 stars measured in the observed area.

Table 1. List of the used frames and exposure times per frame.

Filter	No. Expos.	Exp.Time (sec)	Date
F255W	4	300	April 25,1995
F336W	4	800	April 25,1995
F336W	2	70	April 25,1995
F555W	4	100	April 25,1995
F555W	2	3	April 25,1995
F814W	4	140	April 25,1995
F814W	2	3	April 25,1995

3. The BSS sample from our *HST* observations

As already shown in other UV studies of GGCs (Dorman, Rood, O’Connell 1995 and references therein), the main characteristic of the UV CMD is that at these wavelengths the cluster light is dominated by hot stars, specifically the blue HB stars. The BSS are the next hottest sub-population in the cluster, and are thus easily distinguished from the cooler stars of the turnoff and SGB. The location and morphology of the main branches are very different from the optical CMD. The RGB is very faint, and the choice of ($m_{255}, m_{255} - U$) makes the HB appear diagonal. As can be seen in Figure 2, there is a well-defined, narrow branch extending upward to the left from the giant branch [note however that the choice of the colour frame makes the HB diagonal: the HB is different again in the ($U, m_{255} - U$) plane, almost horizontal]. This branch corresponds to a large part of the HB, excluding the hottest section, which bends downward in m_{255} because of the increasing bolometric correction. The overall morphology of the CMD will be discussed in detail in a future paper (Fusi Pecci et al. 1997), where we will present also a comparison with theoretical models. Here, we only discuss the BSS.

Defining a sample of candidate BSS via photometric techniques is somewhat arbitrary, mostly because of the difficult separation between the faint BSS population and the “normal” MS stars at the TO. We anticipate that, coupled with incompleteness, this problem is one of the main reasons why samples obtained by different observers match so poorly.

To minimize this problem, we have selected the BSS candidates in the UV CMD (m_{255} , $m_{255} - U$). As can easily be seen in Figure 2, in this plane the BSS sequence is quite distinct, spanning ~ 3 mag in m_{255} . To illustrate our selection criteria better, Figure 3 shows a zoomed CMD of the BSS region where the selected candidates are indicated. To reduce the impact of the selection bias on the comparison with previous searches and on the following

discussion, we have divided the total BSS sample into two sub-samples:

1. *bright* BSS: with $m_{255} < 19.0$
2. *faint* BSS: with $19.0 < m_{255} < 19.4$

Since no gap is evident between the BSS sequence and the “normal” stars located in the TO region, we set the limiting magnitude to be $m_{255} = 19.4$ ($\sim 5\sigma$ brighter than the magnitude of the MSTO). The separation between the *bright* and the *faint* samples has been taken to be $m_{255} = 19.0$ in order to be consistent with the limiting magnitude adopted for the two corresponding samples in F93 (see below).

There are several intriguing objects which are clearly located outside the bulk of the population of the main branches and far in colour from the BSS sequence as well. As can be seen from Figure 2, we have not included most of these stars in our sample. They are sometimes called *yellow stragglers* (McClure et al. 1985) as they are intermediate between the blue stragglers and the red subgiants. One should note that they could, and in our view probably do, “contain” a BSS candidate as one component of an *optical* blend with a subgiant (see Ferraro et al. 1992a,b). Even though we are using high resolution *HST* frames some optical blends are still expected because of the high degree of crowding in the very inner regions of M3.

Some similar optical blends are present in almost all CMDs which have been used in the search for BSS candidates, and they have been usually discarded. Therefore, it is conceivable that several BSS are still “hidden” in these optical binaries. Of course, one cannot even exclude that they might be *evolved* BSS (see Ferraro et al 1992a,b for a discussion), but at this stage we adopted the usual definition of BSS and have excluded them from our reported sample.

With the above criteria and caveats, the total number of BSS in our *HST* field is 171. Of these, 72 belong to the *bright* sample and 99 to the *faint*. The two subsamples are plotted with different symbols in Figure 3 (big dots: *bright*; big asterisks: *faint*, respectively). Tables 2 & 3 list the BSS candidates: the first column is our identification number, then in columns 2, 3, 4, 5 we report the V , I , U , m_{255} magnitudes, respectively, and in column 6, 7, 8 the coordinates (X, Y) and the distance (r) from the adopted cluster center in arcsec, respectively¹.

The coordinate system adopted here is the same as used in our previous papers on M3 (F93,PH94,CCD97). A further revision of the whole problem, and a discussion on the choice of an *absolute* reference system is postponed to a forthcoming paper currently in preparation (Laget et al. 1997).

4. Recent searches for BSS candidates in M3

Since a revision and discussion of available ground-based surveys was presented in our previous papers (F93, CCD97), we focus here just on the latest surveys with the goal of achieving a *revised global* sample of BSS in this cluster.

4.1. Ferraro et al. 1993 - (F93)

Based on independent CCD observations at the CFHT and collection and revision of previous data, F93 presented an extensive study of the BSS in M3.

In that study 70 new BSS candidates were identified at $r < 200''$. Coupled with the 76 candidates known from the previous photographic samples (Sandage 1953, Sandage and Katem 1982, Ables et al. 1982, PH94) this yielded the most populous data-set of known BSS in a single GGC. On the basis of this catalog we studied the global BSS radial distribution setting two preliminary constraints:

1. In order to have an homogeneous sample we did not consider candidates in the central region at $r < 20''$ since the sample in that region is likely to be very incomplete in any ground-based photometry, due the high crowding conditions. Moreover, because of inhomogeneity of the surveys, we also excluded the 14 BSS candidates identified at very large distances ($r > 360''$) (Sandage 1953, Ables et al. 1982, see F93 Table 1). Thus, the radial extent of the adopted sample was limited to the range $20'' < r < 360''$.
2. Since the photographic survey was complete to $B = 18.6$, we also limited the analysis only to the bright BSS sample ($B < 18.6$). This choice is surely quite restrictive. On the other hand, as already stressed, the selection of the faint BSS is difficult and quite subjective and may thus introduce significant bias in the analysis.

The main result presented by F93 is reported in their Figure 9: *the relative frequency of the BSS in M3 displays a sharp bimodal radial distribution, with a distinct dip in the region with $100'' < r < 200''$* . However, it was evident that the BSS distribution in the inner regions required much better observations and F93 noted the desirability of additional independent observations.

4.2. Bolte et al. 1993 - (BHS)

Almost simultaneously with F93, Bolte et al. (1993, hereafter BHS) presented the results of a BSS search in M3 carried out using the high-resolution CCD camera at the same telescope (CFHT), but in slightly better seeing conditions. The area covered by BHS is shown in Figure 1 ($\sim 2.2' \times 2.2'$), and overlaps both the previous studies and also our present *HST* survey.

In this very central region, BHS reported the identification of 46 BSS, and defined a *specific frequency* F_{BSS} as

¹ Complete tables 2,3,4 are available on electronic form at the Center de Données de Strasbourg (CDS) and can be obtained by anonymous ftp copy.

the ratio of the number of BSS with respect to those of HB and RGB stars (with $V < V_{\text{HB}} + 2$):

$$F_{\text{BSS}} = \frac{N_{\text{BSS}}}{N(V < V_{\text{HB}} + 2)}$$

In particular, for the central regions of M3 they obtained:

$$F_{\text{BSS}}^{\text{in}} = \frac{46}{1382} = 0.033 \pm 0.005$$

Using the data presented by Paez et al. (1990) on a small external area located at $\sim 375''$ from the cluster center ($r \sim 15r_c$, where r_c is the core radius, i.e., outside the region considered in F93), they obtained:

$$F_{\text{BSS}}^{\text{out}} = \frac{9}{94} = 0.09 \pm 0.03$$

and concluded that the specific frequency of BSS within $5r_c$ of the center of M3 is a factor ~ 2.8 smaller than that seen in the outer regions. If confirmed, this result would be quite surprising and interesting as *none* of the GGCs observed so far has shown a larger frequency of BSS in the outer regions than in the inner ones.

As noted in F93, this result is perhaps somewhat over-interpreted as there was the obvious possibility that their sample could be substantially incomplete in the innermost region of the cluster ($r < r_c$). In this respect, F93 found 14 BSS with $r < 25''$, a number comparable in size to the 19 found by BHS over the same radial interval (see their table 1). However, there were only a few coincidences between the two samples.

CCD97 have further discussed the problem and carried out a detailed comparison between the F93 and BHS samples for $r > 20''$, excluding the innermost region since it required a much better spatial resolution. It has been clear that a reliable revised sample could only be achieved after the analysis of *HST* data.

4.3. Guhathakurta et al. 1994 - GYBS

The first direct confirmation of the large incompleteness of the BHS data came from the first *HST* observations (with WFPC1) of the central regions of M3, before the refurbishment mission. Guhathakurta et al. (1994, hereafter GYBS) presented V ($F555W$) and I ($F814W$) photometry of a $\sim 65'' \times 65''$ region centered $\sim 20''$ E of the commonly adopted cluster center.

They also retrieved U ($F336W$) images from *HST* WF/PC Instrument Definition Team archive which had a small region ($\sim 25'' \times 25''$) in common with their V , I observations (see their Figure 2). Since the (V , $U - I$) plane is more efficient in searching for BSS candidates than the traditional (V , $V - I$) CMD, they restricted their search to only this small overlapping region (namely $r < 20''$). The approximate area of this search is plotted in our Figure 1 together with those of the other surveys. In this area GYBS found 28 BSS candidates.

To better understand the difficulties undermining the detection of BSS in cluster cores, it is quite interesting to note that only half of the 28 GYBS candidates fall in the general BSS area in the BHS CMD, and only 30% actually fall inside the BHS adopted BSS-box (see Figure 10 in GYBS). Moreover, 10 out of 28 GYBS BSS were completely missing in the BHS survey.

As noted by GYBS (see their Figure 9 and 10), from the comparison above, the degree of completeness achieved by BHS in that very central area was less than 25% in the range $V = 17.5 - 18.5$. GYBS also computed the specific frequency of BSS in the central region, yielding:

$$F_{\text{BSS}}(r < 20'') = 28/297 = 0.094 \pm 0.019$$

which is ~ 3 times the value found by BHS, and quite comparable to the BSS frequency they estimated in the outskirts of the cluster.

4.4. Burgarella et al. 1995 - (BPQ)

Burgarella et al. (1995, hereafter BPQ), presented UV ($F220W$, $F346W$) high resolution *HST*/FOC—pre-COSTAR—observations of the core of M3 secured before the repair mission. In the small FOC/96 field of view ($\sim 11'' \times 11''$), they identified 12 BSS and computed the specific frequency which turned out to be:

$$F_{\text{BSS}}(r < 5'') = 12/42 = 0.29 \pm 0.09$$

This figure is three times the value found by GYBS and ~ 10 times that found by BHS. It was thus clear that increasing the spatial resolution of the available observations increases (greatly) the total number of detected BSS candidates.

One has to note that only 5 out of the 12 BSS candidates found by BPQ were also identified as BSS by GYBS, confirming yet again the difficulties in establishing homogeneous the selection criteria. In particular, most of the BPQ BSS candidates are actually close to the TO region (see Figure 3 in BPQ).

5. The BSS specific frequency in the inner regions ($r < 20''$) and comparisons with results from previous surveys

Before computing our independent determination of the BSS specific frequency and carrying out any comparison with the available data-sets, it is important to stress an additional factor which has to be always kept in mind in the analysis and discussion.

5.1. A basic preliminary caveat

From the brief review in Sect. 4 it is evident that, besides the obvious observational problems, the definition of a *reliable and complete* sample of BSS candidates in a GGC is

undermined by the intrinsic uncertainties in the definition of what a *blue straggler* actually is.

Drawing a BSS “box” is highly arbitrary. This problem is clearly evident from the inspection of Figure 9 and 10 in GYBS, and Figure 19a,b in CCD97. In particular, the most critical assumptions concern the separation of the BSS from the “normal” TO and subgiant stars. Furthermore, the BSS selection is strongly dependent on the bands employed in the CMD. In this respect, there is no doubt that long colour baselines (GYBS) and UV filters (BPQ) are preferable.

For this reason we will use our new *HST* sample to compute the BSS specific frequency in the very central regions. Then, using what we have learned, we will construct a *revised global* catalog of BSS candidates in M3 over the complete radial range (see Sect. 6).

5.2. Bolte et al. 1993

As described in the previous section, BHS identified 46 BSS candidates in the very central area. The region covered by our *HST* central field F1 (see Figure 1) overlaps only 75% of the total central zone surveyed by BHS, who have kindly made available to us their data in machine-readable form.

In the region in common, the number of objects listed by BHS is $N_{\text{BSS}}^{\text{BHS}} = 40$ (6 of their candidates located outside our field), while we have $N_{\text{BSS}}^{\text{bright}} = 67$ (and only 4 *bright* BSS candidates are outside the BHS field). Only 30 of all these stars are considered to be BSS in both samples. There are 4 more BHS candidates included in our *faint* sample, and 6 of the BHS BSS have been found to be RGB or SGB stars in our photometry.

In summary, our BSS central population is ~ 1.8 larger than the corresponding one detected by BHS. If we considered as “truly reliable” BSS only the candidates in common between the two searches, the ratio would rise up to 2.2. From this we estimate that the degree of completeness of BHS down to $m_{255} = 19$ is 45–50%.

Turning to the specific frequency of BSS stars as defined by BHS, on our whole *HST*-F1 we have the following results:

$$F_{\text{BSS}} = 72/1140 = 0.06 \pm 0.01$$

while in the region in common with BHS we obtain

$$F_{\text{BSS}} = 67/1099 = 0.06 \pm 0.01$$

This value is almost twice the value obtained by BHS. The difference arises from two (partially compensating) effects. The first, leading to increase F_{BSS} , is the larger number of BSS we detected; the second, leading to decrease F_{BSS} , comes from the higher completeness achieved in the detection of the “normal” reference stars.

Most of the high resolution studies in M3 consider the specific frequency within the innermost region with $r < 20''$, where we get:

$$F_{\text{BSS}}(r < 20'') = 32/290 = 0.11 \pm 0.02$$

And from BHS sample, we find:

$$F_{\text{BSS}}^{\text{BHS}}(r < 20'') = 21/315 = 0.07 \pm 0.02$$

a figure which is surprisingly twice the value they reported on the whole area. Note that using *their* sample and *their* assumptions on the cluster center (485, 689 in their coordinate system), we found 20 BSS with $r < 20''$ and 24 BSS with $r < 25''$ ($= 1r_c$), which is quite different from that listed in their Table 1.

This evidence indicates that in the BHS sample F_{BSS} is much higher in the very innermost region than averaged over the whole sampled area. In particular, we found $F_{\text{BSS}}^{\text{BHS}}(r > 20'') = 26/1071 = 0.024 \pm 0.005$, which is a factor of 3 smaller than that obtained in the inner region.

We can thus conclude that, contrary to their own conclusions, the BHS data already showed a high BSS specific frequency in the very inner regions, even though their achieved completeness was still quite low.

5.3. Guhathakurta et al. 1994

The ratio obtained in the innermost region of M3 ($r < 20''$) from our *HST* sample is compatible with the one found by GYBS. The number of BSS detected in the common area is almost equal at similar magnitude levels (28 by GYBS, 32 in our *bright* sample and 44 in the *faint* one). However, only 24 of these candidates are in common between the two independent selections (19 in the *bright* sample and 5 in the *faint* one, respectively).

5.4. Burgarella et al. 1995

In the small region covered by their FOC/96 observations, BPQ detected 12 BSS. In the same zone, we identified 17 candidates (8 in the *bright* sample and 9 in the *faint* one, respectively) but only 8 (4 in the *bright* sample and 4 in the *faint*, respectively) are in common. We also measured many more “normal” stars so that, though increasing the number of BSS, we actually get a lower F_{BSS} than found by BPQ (if only *bright* BSS are counted):

$$F_{\text{BSS}} = 8/52 = 0.15 \pm 0.08$$

which is still much higher than that obtained by averaging over the total central area. The BPQ selection of BSS candidates has been performed using an UV CMD down to $m_{220} < 19.0$ which is almost coincident with the magnitude ($m_{255} < 19.0$) we adopted to separate the *bright* and *faint* samples. Despite this the final lists are significantly different. This is partially due to the differences in the response of the used cameras (FOC/96 + F220W

and WFPC2 + $F255W$), but it certainly confirms the importance of the photometry and the adopted selection criteria, even starting from quite comparable observational set-ups.

In fact, if we consider our global sample in the region covered by their field we would get:

$$F_{\text{BSS}} = 17/52 = 0.33 \pm 0.08$$

which is fully consistent with the value (0.29) they obtained.

As first noted by BPQ, these values indicate that the BSS specific frequency significantly increases toward the center of M3. Still the small numbers of stars and the residual incompleteness (for both BSS and reference stars) yield an uncertainty large enough to make these values compatible with the F_{BSS} obtained in the whole region with $r < 20''$.

6. The adopted global BSS sample in M3

From the discussion above it is clear that the possible biases affecting any sample of BSS candidates make it quite difficult to produce a *reliable* global catalog of the BSS spanning the complete radial range from the very center out to the far outskirts of M3.

We have therefore decided to collect all the candidates proposed so far by any search and find all the coincidences among the various lists. At this point we adopt general criteria to select a *fiducial* list of BSS candidates. It is not trivial to establish criteria which would give *safe* BSS identifications.

One cannot simply select those stars labeled as BSS in at least two independent surveys, because the different surveys have different resolution and sample different regions of the cluster with different crowding conditions. UV high resolution *HST* data in the central regions yield much more efficient and reliable detections.

In order to make appropriate choices taking into account the above caveats, we adopted different selection criteria in three different zones:

1. The inner region ($r < 20''$), with 4 different surveys (three from *HST*, namely, GYBS, BPQ and this study, and one from the ground, BHS). In this region we have considered as *reliable* BSS candidates only the objects with at least 2 (out of 4 possible) independent identifications.
2. An intermediate region, where *HST* observations (from this survey) and two ground-based surveys (BHS and F93) are available. In this zone we exclude from the *reliable* BSS sample any candidate from ground-based observations which is not confirmed by the *HST* independent search.
3. An additional (quite small) region, with 2 ground based surveys (BHS and F93), but with no *HST* observations for verification. The spatial resolution of these

studies is sufficiently high, considering the much lower degree of crowding at these radial distances from the center, so we accepted all the BSS candidates identified in this region by both surveys.

Table 4 reports the total list of the 263 selected BSS candidates, referred to the same coordinate system (see PH94) and *roughly* to the same photometric system for the V band, eventually applying the magnitude shift (discussed in CCD97) to GYBS and BHS original magnitudes and colours.

The various columns are: (1) the new identification number (in order of increasing distance from the cluster center); (2) the identification numbers (when available) in: this paper (*HST*, Table 2, 3), BPQ, GYBS, BHS, F93, Paez et al. (1990), Ables et al. (1982), Sandage and Katem (1982), and Sandage (1953), respectively; (3) the (apparent) V magnitude adopted to study the BSS luminosity function (note that original magnitudes and colours can be found in each quoted study); (4)-(5) the X , Y coordinates in arcsec; (6) the distance (r , in arcsec) from the adopted cluster center; (7)-(10) the identification labels: numbers indicates the identification numbers in each study in which the BSS has been detected; the label “no” means the BSS candidate is located in the field of view of that survey but it was not identified as a BSS; “out” indicates the BSS is located outside the field of view.

Since there is a large difference in the quality of the sample with decreasing the BSS luminosities, and since we eventually aim at studying the radial distribution of the bright BSS (to avoid strong MS contamination and poor photometry) as we did in our previous study (F93), we have divided also the global sample into two sub-groups, according to the BSS luminosity. In most of the following discussion we will concentrate on the *global bright* sample (whose 122 members are flagged in Table 4).

The *HST* observations of the core of M3 have allowed us to complete the BSS survey over the entire cluster. Since the field covered by the PC is almost exactly the same as that of the data set presented by F93 and CCD97, the main problem we have here is to match the various photometric systems so that the luminosity cuts in the original sub-samples are equivalent. This procedure may have a quite significant impact on the discussion of the radial distribution since, usually, different detectors and photometric systems have been used in different cluster zones.

Using the BSS having all the necessary colours, we have estimated that the limiting magnitude used in F93 ($B = 18.6$) to separate the bright and faint BSS samples corresponds to the magnitude $V \sim 18.3$, and to $m_{255} = 19.0$ used in Sect. 3 to separate the two corresponding *HST* samples. To do this we traced a mean ridge line for the BSS locus in the various CMDs and read the luminosity correspondence at fixed colour. Since the BSS in clusters typically display a wide spread in colour the use of the ridge line would be not strictly justified. How-

ever, we believe that adopting the limits $m_{255} = 19.0$, $B = 18.6$, and $V \sim 18.3$ provides a homogeneous cut with a precision of ± 0.10 mag or better.

6.1. The adopted global bright BSS sample

The 122 BSS brighter than the above magnitude limits (included in Table 4) over the total radial range form our *global bright BSS sample*. In addition, based on the criteria adopted in F93, we have selected samples of reference “normal” stars spanning a similar magnitude interval. These are essentially subgiant branch stars, whose samples should be as complete as the BSS population detected in the same areas, with the same search techniques.

Since the positions of the RGB reference stars in the external region ($r > 360''$) are not available from Sandage (1953), we limited the following analysis to the area within $0\text{--}360''$.

Over this area we have measured V magnitudes (though in different photometric systems from ground-based or *HST* observations) and one or more colours (m_{255} , B and/or I) for almost all these stars. In Figure 4 we plot CMDs in the appropriate colours in different radial regions for both the BSS (*filled triangles*) and reference stars (*dots*). *Panel (a)* shows the $(V, m_{255} - V)$ CMD for the region covered by *HST* – the two lines indicate the limiting magnitudes for the RGB ($B < 18.6$) and the BSS ($m_{255} < 19.0$) samples. *Panel (b)* shows the $(V, V - I)$ CMD for the region with $r < 210''$ and outside the *HST* field. *Panel (c)* shows the $(V, B - V)$ CMD for the outer regions (out to $r < 360''$). In *panel (c)*, 7 bright BSS from Sandage (1953) lying at $r > 360''$ have been plotted as open squares, for completeness. Their original colours have been shifted ($\Delta V = 0.077$ and $\Delta(B - V) = 0.15$) to fit to the BSS sequence.

In Figure 4(a), two bright BSS candidates (namely *No.* 6430 and 35060) have $m_{255} - V > 1.5$; these stars have been found to be strongly contaminated in the V band by nearby ($< 0.2''$) red bright stars.

6.2. The adopted global faint BSS sample

As already stressed, the reliability of the *global faint* sample is low due to the strong selection bias. One should use it with particular care. The present sample gives 141 faint BSS candidates. Their radial distributions in the four annuli considered to describe the *global bright* sample would be 43, 59, 34, 5 at $r < 20''$, $20'' < r < 210''$, $210'' < r < 360''$ and $r > 360''$, respectively. However, since the quality of BSS searching, photometry, and selection is highly variable with distance from the cluster center, we preferred to make no further use of this sample.

7. The BSS radial distribution

As pointed out by many authors and recently summarized by Baily (1995), most BSS in GGCs are found to be centrally concentrated with respect to “normal” stars. Since the central relaxation time in these systems is much smaller than the cluster age, this result is generally ascribed to dynamical mass segregation and interpreted as an evidence that BSS are more massive than the comparison stars. At variance with this simple scenario, in F93 we found that the radial distribution of BSS in M3 is clearly bimodal (see F93, Figure 9).

In this section we discuss first the radial distribution of BSS in the inner regions observed with *HST*, and then extend the analysis to the *global bright* sample spanning the whole radial range. To this aim we have applied the procedure already discussed in our previous papers (see F93, CCD97).

7.1. The BSS radial distribution: the HST central sample

The radial distribution of the 72 *bright* BSS candidates (with $m_{255} < 19.0$) listed in Table 2 has been compared to that of a sample of RGB stars assumed as “reference” population. The BSS have been selected using the m_{255} magnitudes in the UV-CMD, and the RGB stars are much fainter in this band. To compensate for this we checked the reference sample in the $(V, V - I)$ CMD, eventually choosing RGB stars brighter than $V \sim 17$. This procedure reduces the (small) fluctuations introduced by the poorer photometry for the very red stars in the UV bands.

The cumulative radial distributions for the 72 *bright* BSS and the 567 RGB stars are plotted in Figure 5 as a function of their projected distance from the cluster center. It is evident from the plot that the BSS (solid line) are more centrally concentrated than RGB stars (dotted line). In fact, $\sim 50\%$ of the *bright* BSS are inside $r < 24''$ ($\sim 1r_c$), while only $\sim 33\%$ RGB stars are located within this distance.

A Kolmogorov-Smirnov test has been applied to the two distributions to check the statistical significance of the detected difference. The test yields a probability of $\sim 99.5\%$ ($\sim 3\sigma$ level of confidence) that the *bright* BSS population in the central region of M3 has a different radial distribution than the selected RGB stars. The level of confidence grows to $\sim 3.5\sigma$ if one considers the whole sample of 171 (*bright+faint*) BSS listed in Tables 2 and 3.

In conclusion, *there is a significant evidence that the bright BSS candidates are more centrally concentrated than the RGB stars spanning the same magnitude interval.*

7.2. The BSS radial distribution: the global sample

To study the radial distribution of the *global bright* sample, we have compared its cumulative radial distribution with that of the reference stars. The two groups of stars consist of 114 BSS (out of 122) with $r < 360''$ and 1581

RGB stars, and their cumulative radial distributions are reported in Figure 6. As it is evident from the plot and already shown in our previous study (F93, Figure 7), there is a clearly bimodal trend, with the BSS (solid line) more centrally concentrated than RGB stars (dotted line) in the central regions (out to $r < 100''$), while the opposite occurs in the outer regions. Figure 7 reports the cumulative distributions for the data broken into two subsets, separated at $r = 150''$.

Kolmogorov-Smirnov tests applied to RGB and BSS distributions yield the following results for the significance of the difference:

1. global sample ($0'' < r < 360''$): $\sim 99.96\%$ ($\sim 3.5\sigma$)
2. inner sample ($0'' < r < 100''$): $\sim 99.96\%$ ($\sim 3.5\sigma$)
3. outer sample ($100'' < r < 360''$): $\sim 85.5\%$ ($\sim 1.5\sigma$)

These results confirm the existence of a significant dip in the radial distribution worthy of further discussion.

To see this effect in a different way, we have computed the doubly normalized ratios for the BSS and the RGB stars, following the definitions made by F93:

$$R_{\text{BSS}} = \frac{(N_{\text{BSS}}/N_{\text{BSS}}^{\text{tot}})}{(L_{\text{sample}}/L_{\text{tot}}^{\text{sample}})}$$

and

$$R_{\text{RGB}} = \frac{(N_{\text{RGB}}/N_{\text{RGB}}^{\text{tot}})}{(L_{\text{sample}}/L_{\text{tot}}^{\text{sample}})}$$

respectively.

The numbers of BSS and RGB in each annulus, the sampled luminosity, and the resulting ratios with the associated errors are reported in Table 5. The *relative frequency* of BSS so obtained is then plotted as a function of the distance from the cluster center in Figure 8 and compared with the corresponding one for the RGB “reference” stars. Note that an additional annulus with $360'' < r < 600''$ has been added using the candidates by Sandage (1953) to compute R_{BSS} . This annulus gives at least an indication of the BSS population in the outermost parts of the cluster, even though we have no data to compute the corresponding R_{RGB} value.

As can be seen, the BSS specific frequency reaches its maximum at the center of the cluster, showing no evidence of a BSS depletion in the core of M3, contrary to the claim of BHS. We stress that this conclusion has been obtained under the most conservative assumption that only the 32 *bright* BSS detected on the basis of the UV CMD (in the innermost bin) are real.

7.3. Dynamical simulations: comparison with the models

The peculiar radial distribution of BSS in M3 has been the object of a detailed study by Sigurdsson et al. (1994). They presented the results of a simulation of the dynamical evolution of a BSS population in a cluster with structural parameters similar to M3. Sigurdsson et al. assumed

that stellar collisions during interaction in the core of the cluster between (primordial) binary and single stars are the dominant mechanism for the M3 BSS formation. The normalized radial distribution for a sample of ~ 300 BSS obtained from this simulation is overplotted to the observed radial distribution in Figure 9. As noted by Sigurdsson et al. the overall morphology of the simulated distribution is qualitatively identical to the observed one, being able to reproduce:

1. the zone of avoidance at $\sim 5r_c$
2. the rising BSS density for $r > 8r_c$.

This situation arises as follows: the outer BSS have been formed in the core and then ejected into the outer regions by the recoil from the interactions. Those binaries which get kicked out to $r < 7r_c$ rapidly drift back to the center of the cluster due to mass segregation, leading to a concentration of BSS near the center and a paucity of BSS in the outer parts of this region. More energetic kicks will take the BSS to larger distances; these stars require much more time to drift back toward the core and may account for the overabundance of BSS at large distance.

It is quite interesting to note that the simulated BSS density in the innermost radial bin is a sensitive function of the ratio of the BSS lifetime to the halfmass relaxation time which, as noted by Sigurdsson et al. 1994, are highly uncertain. In particular, they set this parameter to a very low value since BHS observations at that time indicated a low BSS density in the core. The new *HST* observations (GYBS, BPQ, and this paper) show a clear overdensity of BSS in the core.

The observed bimodal distribution can provide interesting constraints. Sigurdsson et al. (1994) suggested that it could arise either because the dynamical friction timescale is short compared to BSS lifetime or because the BSS do not receive significant kicks on formation.

8. BSS Luminosity function

Several authors (Bailyn 1992,1995, Aurière et al. 1990, Fusi Pecci et al. 1992,1993, Sarajedini 1993) have suggested that BSS with different origin could have different photometric and spectroscopic characteristics. A potentially fruitful way to check these possibilities is to study in detail the BSS LFs and, in particular, its radial behavior in a cluster like M3 where a bimodal radial distribution has been found.

In particular, we can carry out a *direct* test of the validity of the scenario presented by Bailyn and Pinsonneault (1995–BP95). They computed evolutionary tracks of BSS generated by mergers of primordial binaries and stellar collisions, and presented theoretical LFs for both scenarios, suggesting that BSS made from collisions should be systematically brighter than those made from mergers of primordial binaries.

Even in our first updated BSS catalog (Fusi Pecci et al. 1993), we found quite convincing evidence that the BSS

Table 2. Numbers and relative frequencies for BSS and RGB stars

Annulus	N_{BSS}	N_{RGB}	$L^{\text{sampled}}/10^4 L_{\odot}$	$L^{\text{sampled}}/L_{\text{tot}}^{\text{sampled}}$	R_{BSS}	ϵ_{BSS}	R_{RGB}	ϵ_{RGB}
$0'' - 20''$	32	193	4.0	0.10	2.76	0.27	1.20	0.12
$20'' - 50''$	36	391	8.9	0.23	1.40	0.26	1.09	0.08
$50'' - 100''$	22	376	9.4	0.24	0.81	0.31	1.00	0.08
$100'' - 150''$	3	220	5.7	0.14	0.18	0.67	0.96	0.09
$150'' - 210''$	3	162	4.6	0.12	0.23	0.67	0.88	0.09
$210'' - 290''$	10	128	4.2	0.11	0.82	0.41	0.76	0.09
$290'' - 360''$	8	111	2.6	0.07	1.06	0.45	1.06	0.13

LFs for clusters with $\log \rho_o < 3$ and $\log \rho_o > 3$, respectively, seem to be different (at more than 3σ). This earlier result supported the hypothesis that the BSS formation mechanism varies with varying overall cluster structural properties. It is thus quite easy to compare the available BSS data with the LFs predicted by BP95.

Since the theoretical LFs computed by BP95 are given in bolometric luminosity, a correction must be first applied to the data before comparing them with their models. Assuming for the absolute magnitude of the TO level $M_V = 4.0$ and a differential Bolometric Correction equal to 0.1 mag between the BSS and the TO stars, following BP95, we computed for each star the quantity:

$$\text{Log}(L/L_{\text{TO}}) = 0.4(3.9 - M_V)$$

In Figure 10 we compare the BSS LFs for high density clusters (*panel a*) and low density clusters (*panel b*), respectively, with the corresponding theoretical LFs. The BSS LF for low-density clusters appears to be consistent with that predicted from the merging of primordial binaries, while the BSS LF for high-density clusters fits better to the claim that they were mostly formed by collisions. Though not conclusive—both the available data and the models need to be improved—this comparison adds some observational support to the claim that BSS formation mechanisms are affected by environmental conditions.

We can now test further this idea and the model proposed by BP95 by using the available BSS catalog in M3 to compare the BSS LFs obtained from different radial areas. In fact, as pointed out first in our previous paper (F93), the bimodal BSS radial distribution in M3 naturally leads one to imagine that the BSS located in the inner regions of the cluster could have a different origin with respect to those populating the outer zones.

Following this suggestion and using the BSS sample we published in F93, BP95 found convincing evidence that the BSS in the outer regions of M3 were probably formed from mergers of primordial binaries. They were however

unable to reach firm conclusions concerning the innermost regions ($r < 20''$), where the sample was very small and covered a restricted luminosity range (in order to avoid the contaminations from supra-SGB stars). The *HST* data give us the opportunity to further investigate this aspect.

Therefore, we have obtained the LFs for the BSS (a) located within the region $0'' < r < 100''$ from the cluster center (see Figure 8) and with $B < 18.6$, and (b) located within the annulus with $210'' < r < 360''$. Following BP95, we have adopted:

$$\text{Log}(L/L_{\text{TO}}) = 0.4(19.1 - V)$$

and computed the LFs over luminosity bins of 0.1 (= 0.25 mag).

In Figure 11 the observed BSS LFs in the two regions are compared to the theoretical ones obtained from the BP95 models. The observed LF in the inner region is clearly compatible with that predicted within the collisional framework, while that obtained in the outer annulus is consistent with the prediction of primordial binaries merging.

As noted above, for the comparisons of the BSS LFs of different clusters, these indications are still too crude to allow us to draw any firm conclusion based on a complete statistical analysis. However, in our view this evidence confirms the possibility that two different populations of BSS can actually be present in M3.

8.1. Special warning

Concerning the possible interpretation of the global BSS properties (i.e. radial distribution and LF), we have to note that the comparison with the (still uncertain) theoretical models would yield a possible contradicting scenario. In fact:

- (a) the radial distribution (see section 7.3) fits properly to the Sigurdsson et al. (1994) model, which suggests that all BSS are formed via collisions in the central

area and only a fraction of them are kicked out at large distance;

- (b) the LFs seem to be in agreement with the BP95 models which would lead to interpret the whole BSS population as formed by two main mechanisms: collisions (in the inner regions) and merges of primordial binaries (in the outer regions).

We cannot solve the *dilemma* on the basis of the available data. Spectroscopic information could perhaps add useful hints on the issue. In particular, data on the detailed chemical abundances (especially, helium) and on rotational velocities could set important constraints on modeling the BSS formation and evolution.

9. Evolved BSS on the HB?

Renzini and Fusi Pecci (1988) first suggested that some stars located at the red extreme of the HB could be *evolved* BSS, experiencing the core helium burning phase. Then, assuming a binary origin for the BSS (which, in turn, leads them to have high masses) and using the models computed by Seidl et al. (1987), Fusi Pecci et al. (1992) identified 47 red HB objects as possible post-BSS candidates in a sample of 10 GGCs. In particular, Renzini and Fusi Pecci (1988) identified 7 stars in M3 slightly brighter and redder than *normal* HB stars which could represent the evolved-BSS population.

To pursue this idea in our subsequent studies of M3, we (PH94, CCD97) defined a photometric box suitable to identify these post-BSS candidates, labeled as ER (Extreme Red)-HB stars. Now, based on the whole PHOTO+CCD+HST sample which we have secured, we estimate the total ER-HB population to be 19 stars. For clarity, we have plotted a zoomed CMD of the HB in Figure 12, and the box delimiting the ER stars in HB has been shown.

Having defined a set of “plausible” post-BSS candidates, one can then check whether these stars have retained memory of the unusual radial distribution of their progenitors.

Unfortunately, the ER sample is *intrinsically* quite poor, so we have defined only 4 radial bins instead of 7, and have computed the double-normalized frequency (R_{ER}) as defined for the BSS:

$$R_{ER} = \frac{(N_{ERanul}/N_{ERtot})}{(L_{anul}/L_{tot})}$$

Where N_{ERanul} , L_{anul} , N_{ERtot} , and L_{tot} are the numbers of detected ER-HB stars and the sampled luminosity in each annulus, and the total sample respectively.

In Figure 13 *panel a*, the relative frequency of ER-HB stars in M3 is plotted as a function of the radial distance from the cluster center, while *panel b* shows the radial behavior of the BSS. As can be seen the overall trend is qualitatively the same, and the region with $100'' < r < 200''$

characterized by a depletion of BSS shows a clear deficit of ER-HB stars too. The statistical significance of this depletion is admittedly poor since only 3 stars have been detected compared to the 10 expected in the region of the dip. The observed number is only a $\sim 2\sigma$ fluctuation from the expected value. Clearly it is too speculative to conclude that we have shown the existence of a true connection between the ER-HB stars and the BSS. On the other hand, it may be useful for future analyses to keep track of such a clear qualitative agreement between the two radial distributions.

If one assumes that the connection between the ER-HB stars and the BSS is real, one can relate the population ratios and the lifetimes of these evolutionary stages. The ratio between the number of BSS and ER-HB stars using our sample in M3 ($r < 360''$) is

$$\frac{N_{BSS}}{N_{ER-HB}} = \frac{122}{19} = 6.4$$

which is in good agreement with a mean value of 6.6 over a sample of 10 GGCs found by Fusi Pecci et al. (1992).

For comparison, Greggio & Renzini (1990) give a relation for the expected number of ER-HB as a function of the sampled luminosity on the basis of the so-called fuel consumption theorem (Renzini and Buzzoni 1986) yielding:

$$N_{ER-HB} = 6 \times 10^{-13} L_T t_j$$

Assuming $t_{HB} \sim 10^8$ yr from Seidl et al. (1987) and considering that with the complete PHOTO+CCD+HST survey we have sampled $\sim 4 \times 10^5 L_{\odot}$ (i.e. $\sim 77\%$ of the whole cluster luminosity), we have that the predicted number of ER-HB stars would be $N_{ER-HB} \sim 24$, which is in excellent agreement with our observed sample (19 stars). However, first, one has to note that the above relation for the lifetime has actually been calibrated using the population of BSS and ER-HB in the outer regions of M3 (Buonanno et al. 1986), so this result cannot really be considered to be an independent confirmation of the connection between the two stellar populations. Second, the fuel consumption theorem may well not apply to BSS straightforwardly, since they probably start out with considerable fuel already burned in their cores.

Despite the care we have taken, the connection of ER-HB stars with the post-BSS is “suggestive” rather than proven. We think it is worthwhile to pursue the detailed search and study of the post-BSS since they *must* be detectable *somewhere* in the CMD of any GGC containing BSS (Renzini and Fusi Pecci 1988, Fusi Pecci et al. 1992). The HB is still the most promising location where they could be identified as (if truly more massive) they could somehow differ from “normal” cluster stars. On the other hand, if correct, our previous estimate indicates that to detect 1 post-BSS during the core helium burning phase (ER-HB), one must sample $\sim 2 \times 10^4 L_{\odot}$. This implies

that in order to obtain a statistically significant sample of ER-HB stars one should sample large fractions ($> 50\%$) of the brightest GGCs.

Given the difficulty of observing samples adequately large to connect the ER-HB and post-BSS via population studies, it might be appropriate to consider alternate techniques. In either the merged binary or collision mechanisms one might expect a substantial amount of CNO processed material to end up in the surface layers of the stars. This material could show the same kind of abundance anomalies found by Kraft et al. (1996 and references therein) in highly mixed red giants, i.e., extreme oxygen depletion coupled with sodium and aluminum enhancements. A differential study comparing ER-HB/post-BSS candidates to normal RHB stars could be quite revealing.

10. Variable BSS in M3

Mateo et al. (1996 and references therein) have shown the existence of variable BSS and classified them as SX Phoenicis, eclipsing binaries or contact binaries W UMa.

Our observations do not have a time coverage suitable to look for variability. It is thus difficult to select BSS variable candidates only on the basis of our photometry. Since the U exposures cover ~ 25 minutes in time duration, possible BSS candidates can be perhaps found by looking for particularly large values of σ_U , the rms frame-to-frame scatter.

The mean σ_U in the range of magnitude $17.5 < U < 18.5$ for the RGB stars and for BSS is $\sigma_U^{RGB} = 0.02$. It is quite interesting to note that BSS/5866 shows a $\sigma_U \sim 0.16$ which is $\sim 8\sigma$ greater than the average value; this BSS has not been catalogued as possible variable by GYBS, who, on the other hand, found only one variable BSS in their sample: BSS/576 (in their catalog). For this star they published also a possible light curve (see figure 16 in GYBS), however in our photometry this star –BSS/1498– has $\sigma_U = 0.033$. It is thus hard to say any additional comment on variability.

11. Three very bright BSS in M3

Figure 14 shows the CMD in the ultraviolet plane with the total sample of BSS identified using different symbols (*big dots* = bright BSS, and *asterisks* = faint BSS). Overplotted on the data are two isochrones (2 and 14 Gyr) computed by Dorman (1995, unpublished). These respectively have a TO-mass of ~ 0.8 and $\sim 1.5 M_\odot$. Most of the BSS candidates are consistent with a mass $< 2M_{TO}^{M3}$, and are thus clearly compatible with the hypothesis that they are the result of advanced stages of evolution of binary systems.

However, it is also quite interesting to note that there are three objects which are ~ 0.5 mag brighter than the predicted TO of the $1.5M_\odot$ track. None of these (namely

No. 24768, 50012 and 6674) were present in the selection by BHS and GYBS. Two (No. 24768 and 6674) are actually brighter (0.3 mag) than the BSS box defined by BHS, and are located slightly fainter than the blue region of the HB. No. 6674 is located within the field covered by GYBS, but it was not considered to be a BSS candidate. The third object (No. 50012) is an HB star in BHS and F93 while it is outside the field covered by GYBS. Since this object is positioned in our frames very close to the WF2 edge, we cannot exclude the existence of a sizable error in our photometry, and will thus exclude it from the following analysis.

The positions of these stars in the UV-CMD suggest that they could be bright BSS rather than “peculiarly faint” HB stars, since the HB is quite well defined and these stars are located ~ 0.5 mag below the lower envelope of the HB (the plausible Zero Age HB). Since they do not show any variability, they cannot be identified as candidate RR Lyrae variables observed out-of-phase in the two colours. If they are “true” BSS, these objects could have originated from multiple systems (3 or more objects), and would demonstrate that such complex interactions can take place in the core of M3.

The possible formation of multiple systems has been proposed by Leonard (1993) from the interaction between two binary systems. Their existence could, for instance, explain the BSS F81 in M67, which shows a mass greater than twice the TO mass (Leonard and Linnel 1992). The predicted percentage of the “stable” multiple systems from collision of binary systems is $\sim 2-4\%$ (Leonard 1996), fully compatible with our observed percentage ($3/171 \sim 2\%$).

Alternatively, the very high luminosity reached by the brightest BSS could be ascribed to the effects of helium mixing in the envelope during the collision. In particular, Sandquist et al. (1997) describe the evolution of massive objects obtained from hydrodynamical simulations of direct collisions of single and binary stars. They suggested that the luminosities of the brightest BSS (much brighter than expected for a $2 M_{TO}$ star) can still be explained by the merger of two $1 M_{TO}$ stars. The resulting object has overall helium enrichment because the collision mixes the helium produced during the prior evolution.

12. Conclusions

Using new *HST* observations and a thorough revision of all previous surveys of blue straggler stars in M3, we carried out a complete re-analysis of BSS properties and, in particular, of their radial distribution. The results are:

- From the careful revision of all the 263 BSS candidates proposed at least by one of the various surveys carried out so far, we have adopted an updated catalog of the BSS candidates in M3 which includes 122 *bright* (with $B < 18.6$, $V < 18.3$, $m_{255} < 19.0$) and 141 *faint* objects. The *bright global* sample within the radial region at $0'' < r < 360''$ includes 114 objects. This

sample, hopefully complete over the whole region, has been used for the subsequent analysis. All the candidate objects are listed along with comments in Table 4. The *faint* sample is surely incomplete and it may be strongly biased by the selection criteria which are hard to define at the separation between the BSS region and the MS stars.

- The BSS radial distribution is clearly peaked at the cluster center. BSS candidates in the inner regions (see section 7.1) are more concentrated than “reference” normal SGB and RGB stars. In particular, star counts yield a rather high specific frequency for the BSS in the cluster core, contrary to previous claims which were affected by incomplete samples.
- The global radial distribution of the BSS in M3 is bimodal, with a clear-cut dip in the region at $100'' < r < 200''$ and a rising trend in the outer region (out to $r \sim 360''$), as first noted by F93. This evidence adds support to the idea that different mechanisms of BSS formation and survival could be at work also within the same cluster, or that special segregation effects take place during the dynamical cluster evolution. There is an interesting *qualitative* agreement between the observed radial distribution of the *bright* BSS and the predictions of the dynamical models computed by Sigurdsson et al. (1994) which take into account both star collisions and merging of primordial binaries.
- The total Luminosity Function is consistent with that obtained for all the known BSS candidates (about 700 in ~ 35 GGCs, see Fusi Pecci et al. 1992, Sarajedini 1993, Bailyn 1995). Due to quoted selection biases, the faint end of the LF is still highly uncertain. In addition, as already found in other clusters (see references above), there are a few BSS candidates which seem too bright to possibly have originated from binary systems.
- The LFs of the inner ($r < 100''$) and outer ($r > 210''$) regions are different. The brightest BSS are slightly more frequent in the central zones. In particular, comparing with the available models (BP95), one finds that the BSS LF in the outer regions ($r > 210''$) is consistent with the scenario based on merging of primordial binaries as basic formation mechanism. In the central region, the BSS LF is compatible with the collisional origin, though the significance of the difference is small.

From the above considerations, the BSS content in M3 can be schematically described as follows:

1. A large fraction of the BSS populate the very central cluster regions. The LF suggests that most of them were probably generated by stellar collisions (possibly) involving primordial binaries, which are actually disrupted in the core (BP95).
2. The dip detected in the radial distribution is probably due to mass segregation. In particular, according to Sigurdsson et al. (1994), primordial binaries lying less than $7r_c$ from the cluster center are attracted toward the center and then disrupted, and BSS produced by collisions in the core and kicked out at $r < 7''$ drift back to the core in a short time-scale.
3. On the other hand, most of the BSS in the outer regions are originated from the merging of primordial binaries, though a few of them could also be originated by collisions in the core and pushed out at large distances because of very energetic dynamical kicks (Sigurdsson et al. 1994).

A deeper discussion of the BSS properties in this and in other GGCs will be surely possible as soon as new data will become available from the *HST* frames currently taken or reduced for the central regions of many Galactic globular clusters.

Acknowledgements. We gratefully thank the referee, Charles Bailyn, for helpful comments and suggestions to improve the presentation, and G. Iannicola and I. Ferraro whose expertise on ROMAFOOT was invaluable for the completion of this work. This research was supported by the *Ministero dell' Università e della Ricerca Scientifica e Tecnologica* (MURST), the *Agenzia Spaziale Italiana* (ASI), and the *Gruppo Nazionale di Astronomia del Consiglio Nazionale delle Ricerche* (GNA-CNR). R.T.Rood & B.Dorman are supported in part by NASA Long Term Space Astrophysics Grant NAGW-2596.

References

- Ables, H.D., Dahn, C.C., & Hewitt, A.V. 1982, *PASP*, 94,748
Aurière, M., Ortolani, S., Lauzeral, C., 1990, *Nature*, 344, 638
Bailyn, C.D., 1992, *ApJ*, 392, 519
Bailyn, C.D., 1995, *ARA&A*, 33, 133
Bailyn, C.D., Pinsonneault, M.H., 1995, *ApJ*, 439, 705 (BP95)
Bolte, M., Hesser, J.E., Stetson, P.B. 1993, *ApJL*, 408, L89 (BHS)
Buonanno, R., Corsi, C.E., Buzzoni, A., Cacciari, C., Ferraro, F.R., Fusi Pecci, F. 1994, *A&A*, 290, 69 (PH94)
Buonanno, R., Buscema, G., Corsi, C.E., Ferraro, I., Iannicola, G. 1983, *A&A*, 126, 278
Buonanno, R., Buzzoni, A., Corsi, C.E., Fusi Pecci, F. Sandage, A.R. 1986, *Mem.SAIt*, 57, 391
Buonanno, R., Corsi, C.E., De Biase, G.A., Ferraro, I. 1979, in *Image Processing in Astronomy*, eds. G. Sedmak, M. Cappacioli & R.J. Allen, Trieste, Italy, p.354
Buonanno, R. & Iannicola, G. 1988, *PASP*, 101, 294
Burgarella, D., Paresce, F., Quilichini, V. 1995, *A&A*, 301, 675 (BPQ)
Dorman, B., Rood, R.T., O'Connell, R. 1995, *ApJ*, 442, 105.
Ferraro, F.R., Fusi Pecci, F., Buonanno, R., 1992a, *MNRAS*, 256, 376
Ferraro, F.R., Clementini, G., Fusi Pecci, F., Sortino, R., Buonanno, R., 1992b, *MNRAS*, 256, 391
Ferraro, F.R., Bellazzini, M., Fusi Pecci, F., 1995, *A&A*, 294, 80
Ferraro, F.R., Fusi Pecci, F., Cacciari, C., Corsi, C., Buonanno, R., Fahlman, G.G., Richer, H.B. 1993, *AJ*, 106, 2324 (F93)
Ferraro, F.R., Carretta, E., Corsi, C., Fusi Pecci, F., Cacciari, C., Buonanno, R., Paltrinieri, B., Hamilton, D., 1997, *A&A*, in press (CCD97)

- Fusi Pecci, F., et al. 1997, in preparation
- Fusi Pecci, F., Ferraro, F.R., Cacciari, C., 1993, in *Blue Stragglers*, ed. R.A. Saffer, ASP Conf. Series, 53, 97
- Fusi Pecci, F., Ferraro, F.R., Corsi, C.E., Cacciari, C., Buonanno, R. 1992, *AJ*, 104, 1831
- Greggio, L., Renzini, A. 1990, *ApJ*, 364, 35
- Guhathakurta, P., Yanny, B., Bahcall, J.N., Schneider, D.P. 1994, *AJ*, 108, 1786 (GYBS)
- Holtzmann, J.A., Burrows, C.J., Casertano, S., Hester, J.J., Trauger, J.T., Watson, A.M., Worthey, G., 1995, *PASP*, 107, 1065
- Kraft R.P. et al. 1996, *AJ*, 109, 2586
- Laget et al, 1997, in preparation
- Leonard, P.J.T., Linnel, A.P., 1992, *AJ*, 103, 1928
- Leonard, P.J.T., 1993, in *Blue Stragglers*, ed. R.A. Saffer, ASP Conf. Series, 53, 189
- Leonard, P.J.T., 1996, in *The origins, evolution and destinies of binary stars in clusters*, eds. E.F. Milone and J.C. Merrelliod, ASP Conf. Series, 90, 337
- Mateo, M. 1993, in *Blue Stragglers*, ed. R.A. Saffer, ASP Conf. Series, 53, 74
- McClure, R.D., Hesser, J.E., Stetson, P.B., Stryker, L.L., 1985, *PASP*, 97, 665
- Paez, E., Straniero, O., Martinez Roger, C. 1990, *A&AS*, 84, 481
- Renzini, A., Buzzoni, A. 1986, in *Spectral Evolution of Galaxies*, C. Chiosi and A. Renzini eds., (Reidel, Dordrecht), 135
- Renzini, A., Fusi Pecci, F. 1988, *A.R.A.&A.*, 26, 199
- Sandage, A.R. 1953, *A.J.*, 58, 61
- Sandage, A.R., Katem, B. 1982, *A.J.*, 87, 537
- Sandquist, E.L., Bolte, M., Hernquist, L., 1997, *ApJ*, March issue.
- Sarajedini, A. 1993, in *Blue Stragglers*, ed. R.A. Saffer, ASP Conf. Series, 53, 14
- Seidl, E., Demarque, P., Weinberg, D., 1987, *ApJS*, 63, 917
- Sigurdsson, S., Davies, M.B., Bolte, M., 1994, *ApJ*, 431, L115

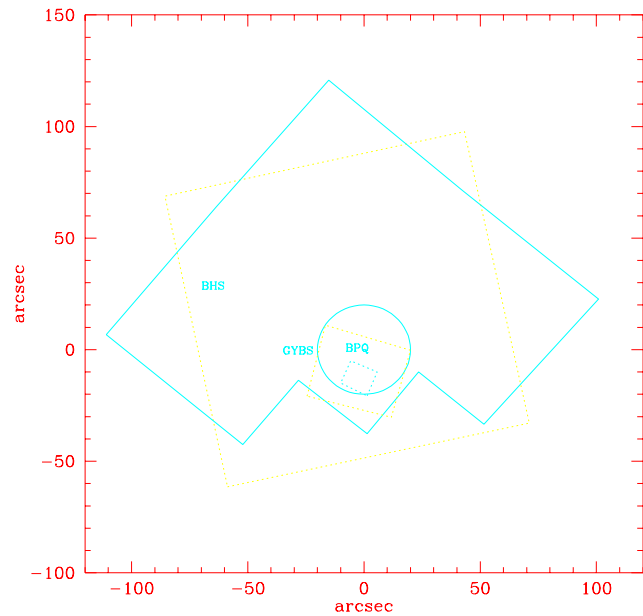


Fig. 1. The areas surveyed in various BSS studies of M3. The global (PC+WF2+WF3+WF4) field of view of the *HST* field is shown by the solid line. The dotted squares represent the boundaries of previous surveys in the center of M3: Bolte et al. (1993, labeled BHS), Guathakurta et al. (1995, label GYBS), Burgarella et al. (1995, labeled BPQ), respectively. The circle at $r = 20''$ is the inner limit of our previous ground-based surveys (F93, CCD97).

Fig. 2 Converted to .jpg file

Fig. 2. UV-CMD in the plane (m_{255} , $m_{255} - U$) for more than 18,000 stars identified in the *HST* field. The variable stars are not shown.

Fig.3 converted to .jpg file

Fig. 3. Blue stragglers in M3. The solid line at $m_{255} = 19.4$ is the assumed limiting magnitude (which is $\sim 5\sigma$ above the TO level). The dashed line at $m_{255} = 19.0$ (which corresponds to $B \sim 18.6$ in PH94) divides the total sample in two sub-samples: the Bright sample (Bright-BSS) *solid circles* and the the Faint sample (Faint-BSS) *asterisks*

Fig. 4 converted to .jpg file

Fig. 4. The BSS candidates (filled triangles) in different parts of the cluster, and the RGB (dots) population for comparison. *Panel (a):* the (V , $m_{255} - V$) CMD for the region covered by *HST* – the two lines indicate the limiting magnitudes for the RGB stars ($B < 18.6$) and the BSS ($m_{255} < 19.0$); *panel (b):* the (V , $V - I$) CMD for the region with $r < 210''$ outside the *HST* field; and *panel (c):* the (V , $B - V$) CMD for the outer regions (to $r < 360''$). In panel (c) the empty squares are 7 bright BSS from Sandage (1953) with $r > 360''$: their original colours have been shifted ($\Delta V = 0.077$ and $\Delta(B - V) = 0.15$) in order to fit to the BSS sequence.

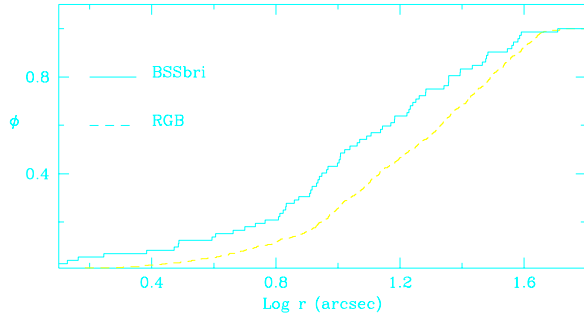


Fig. 5. Cumulative distribution of the Bright-BSS (full line) and the RGB stellar population (dashed line) in the *HST* field.

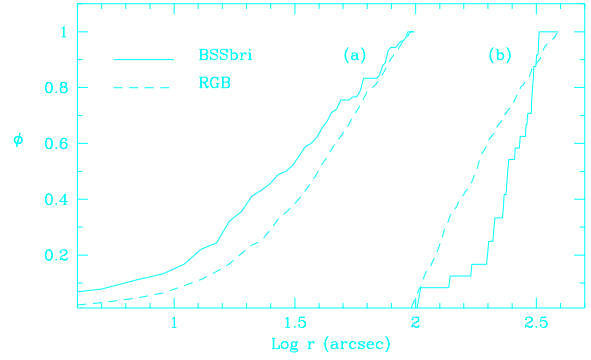


Fig. 7. Same as Figure 5 for the sub-sample of stars at (a) $r < 2.5'$ and (b) $2.5' < r < 6'$.

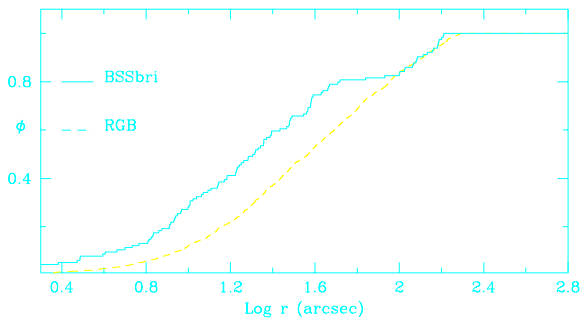


Fig. 6. Same as Figure 5 over the distance range $0 - 6'$.

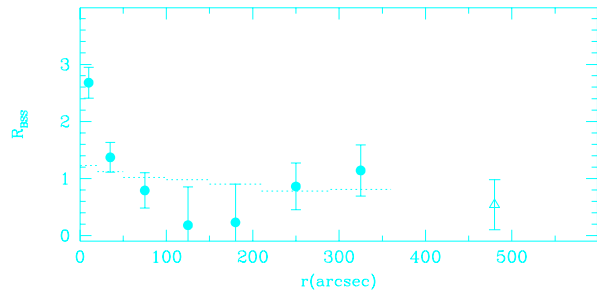


Fig. 8. The relative frequency of BSS in M3 is plotted as a function of the radial distance from the cluster center. The horizontal lines show the relative frequency of the RGB stars used as a comparison population. Note that for $r > 6'$ only the relative frequency of BSS has been computed using the Sandage (1953) candidates.

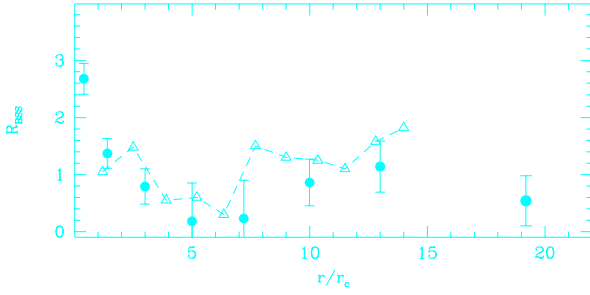


Fig. 9. The relative frequency of BSS in M3 is plotted as function of the radial distance from the cluster center in units of core radii. The frequency expected from the simulation by Sigurdsson et al. (1994) has been overplotted as empty triangles.

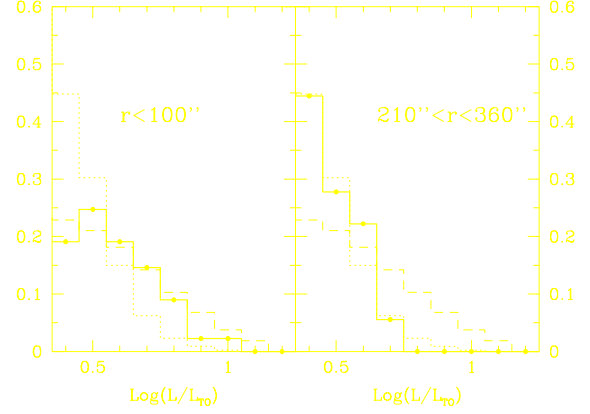


Fig. 11. The BSS luminosity functions for the inner regions ($r < 100''$ – panel (a)) and outer regions ($r > 210''$ – panel (b)) are compared to the theoretical predictions: line symbols have the same meaning as in Figure 9.

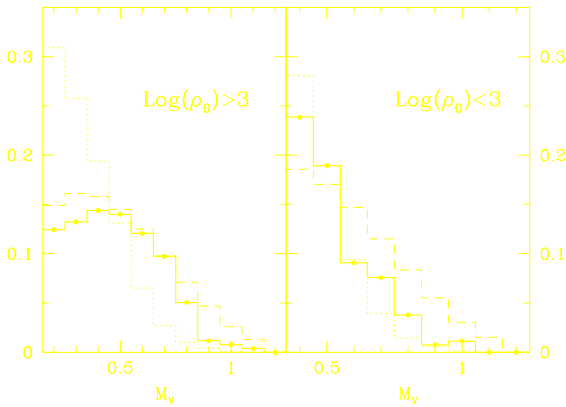


Fig. 10. The BSS luminosity functions (solid lines) for clusters having $\log(\rho_0)$ greater and smaller than 3 (panels (a) and (b), respectively) are compared to the theoretical LFs for collisional BSS (dashed line) and primordial binary merger BSS (dotted line). The data are from Fusi Pecci et al. (1993), the theoretical LFs are from BP95.

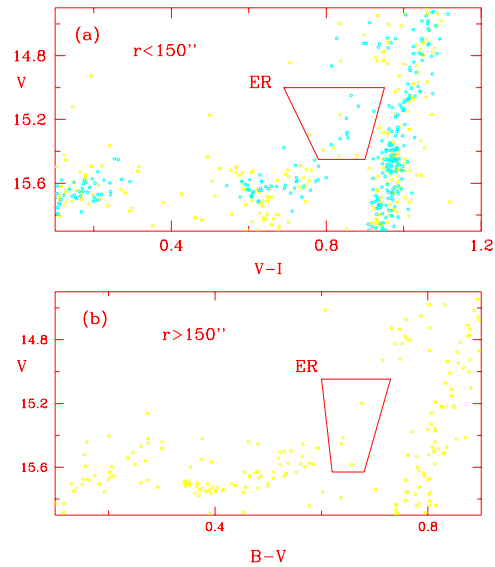


Fig. 12. Zoomed CMD of the Horizontal branch region. The box defines the area in which the BSS progeny are expected (see PH94, CCD97). Panel (a): $(V, V - I)$ CMD for stars at $r < 150''$; panel (b): $(V, B - V)$ CMD for stars at $150'' < r < 360''$ and outside the *HST* field.

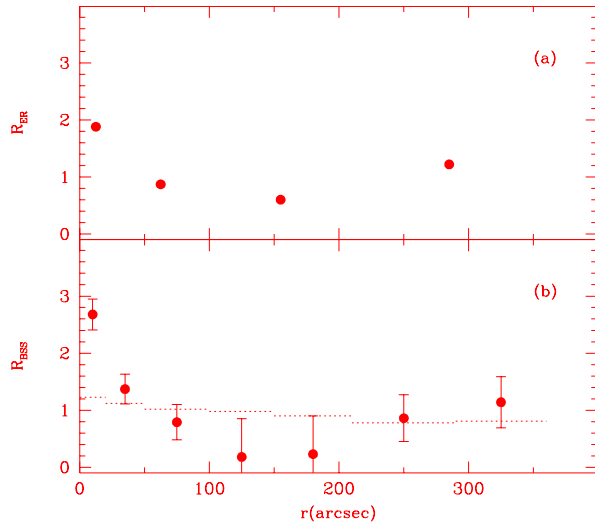


Fig. 13. *Panel (a)* The relative frequency of ER-HB stars in M3 is plotted as function of the radial distance from the cluster center. *Panel (b)* The relative frequency of the BSS is plotted for comparison. As can be seen the overall trend for the two types of star is qualitatively the same.

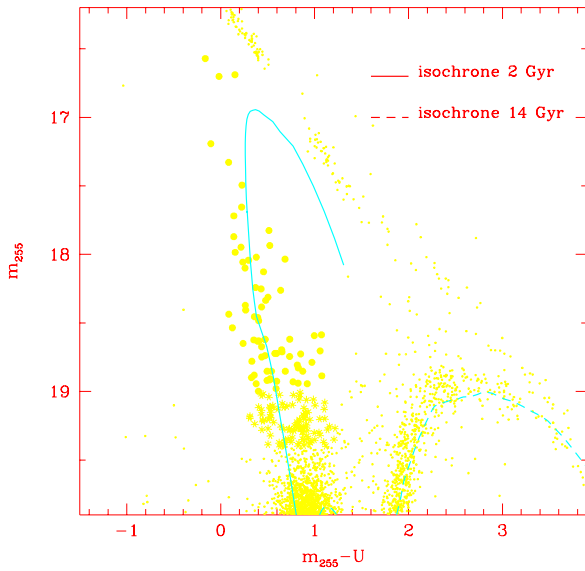


Fig. 14. Zoomed CMD of the BSS region: the symbols have the same meaning as in Figure 3. Two isochrones have been plotted: (i) 14 Gyr (dashed line) with a TO mass of $\sim 0.8M_{\odot}$ which nicely fits to the TO region and the RGB; and (ii) 2 Gyr (solid line) which corresponds to a TO mass of $\sim 1.5M_{\odot} \sim 2 \times M_{TO}$ (Dorman 1995, unpublished).

Tab.2 HST BSS : bright sample

Tab.2 (continued)

N	V	I	U	m_{255}	X	Y	N r	V	I	U	m_{255}	X	Y
7821	18.176	17.748	18.389	18.979	-1.040	0.610	2101820618.014	17.439	17.432	17.655	-22.850	5.4	
5866	17.863	17.441	18.151	18.622	-1.750	1.230	4708113917.998	17.820	18.224	18.631	8.760	23.1	
5906	17.510	17.303	17.841	18.100	-2.680	-0.190	318068717.887	17.536	18.146	18.723	-11.070	-23.0	
7785	17.963	17.820	18.271	18.624	-1.110	-2.690	152491017.398	17.100	17.745	18.042	0.470	-27.4	
6674	16.593	16.507	16.735	16.571	2.210	2.740	353352017.864	17.597	18.080	18.484	-1.940	27.7	
6430	17.310	16.677	17.809	18.886	-1.930	-4.430	4816483217.437	16.808	17.645	18.704	28.250	9.0	
5981	18.016	17.435	18.311	18.748	-2.750	-5.260	3078493518.167	...	18.351	18.437	-3.720	30.1	
3736	17.801	17.650	18.096	18.455	6.050	1.060	2127014217.516	17.583	17.732	17.871	-30.470	-1.4	
7678	17.028	16.941	17.243	17.328	-6.060	-0.870	4747012217.609	17.472	17.822	18.252	32.350	-8.3	
6318	18.166	17.984	18.412	18.650	-1.040	7.790	3537085918.283	17.954	18.524	18.881	6.870	33.1	
7850	18.308	18.006	18.411	18.535	-3.810	-7.120	3378407517.555	17.408	17.870	18.241	-5.540	33.7	
6979	17.557	17.436	17.831	17.985	9.070	-1.470	50092188	...	16.537	16.689	-30.240	-17.4	
5313	17.637	17.005	18.022	18.944	9.670	-2.620	23170401917.934	...	18.238	18.673	-30.510	18.4	
6352	17.799	17.552	18.109	18.371	9.720	-4.800	470284117.045	17.109	17.267	17.494	36.470	2.7	
7069	17.284	16.953	17.641	18.020	1.940	-11.490	4581065317.305	16.628	17.595	18.592	26.630	27.6	
2926	17.082	16.970	17.297	17.192	-8.150	-9.960	23512841018.195	17.645	18.359	18.853	-31.800	21.4	
1769	16.989	16.448	17.350	18.035	-0.940	-12.960	232199417.078	16.819	17.412	17.935	-43.830	2.7	
47750	17.734	17.860	17.821	18.056	-1.030	13.280	237432017.838	17.187	18.116	18.940	-44.550	8.7	
47934	18.114	...	18.311	18.852	10.070	9.090	4463056618.461	16.755	18.571	18.899	40.320	-21.1	
2444	17.655	17.035	17.991	18.807	-9.140	-10.120	3470463617.675	17.034	17.874	18.726	13.930	43.3	
1855	18.133	17.637	18.426	18.919	-7.430	-12.430	3195648117.443	16.752	17.816	18.787	7.940	48.9	
48425	18.294	17.995	18.393	18.915	9.640	11.420	2476894516.628	16.553	16.720	16.702	-38.720	30.9	
20075	17.516	17.174	17.810	18.313	-12.860	9.880	3416721718.107	...	18.330	18.926	3.410	54.1	
45876	17.691	...	17.948	18.384	15.970	3.520	3216035317.340	16.859	17.624	18.262	2.950	58.4	
1244	18.451	18.202	18.566	18.944	-0.120	-16.510	206751017.843	...	18.046	18.695	-50.870	-31.5	
3407	17.434	17.251	17.732	17.948	-11.740	-12.370	2547405418.326	17.969	18.596	18.998	-55.240	24.1	
48119	17.657	17.166	18.002	18.829	8.490	15.030	246826218.202	...	18.448	18.780	-60.880	2.8	
2922	17.731	17.242	18.011	18.745	-17.310	-1.870	2187341118.075	...	18.382	18.908	-61.720	-33.8	
7698	17.426	16.924	17.671	18.127	11.840	-13.220	234774717.870	17.718	18.140	18.406	-68.590	-24.1	
1441	17.918	17.305	18.266	18.739	-6.750	-17.110	243839317.667	17.139	17.884	18.619	-71.860	-16.3	
519	17.908	17.575	18.240	18.633	-16.200	-9.070	265856617.824	17.413	18.066	18.460	-63.710	41.6	
1498	16.918	16.534	17.312	17.826	-8.610	-17.960	3506091716.856	16.132	17.513	18.586	-5.500	76.7	
4032	17.857	17.299	18.128	18.723	15.340	-13.080	2620215917.288	17.309	17.579	17.719	-76.680	14.6	
5214	17.867	17.272	18.165	18.853	19.200	-6.880	2620239517.739	17.116	17.979	18.853	-101.480	11.8	
47269	18.005	17.657	18.146	18.619	3.760	20.010	20.360						
46285	17.879	17.762	18.058	18.711	18.550	9.900	21.026						
21131	17.908	17.458	18.160	18.930	-17.040	13.700	21.864						
35187	17.668	17.354	17.858	18.336	-8.090	21.600	23.065						

Tab.3 HST BSS : faint sample

Tab.3 (continued)

N	V	I	U	m_{255}	X	Y	Nr	V	I	U	m_{255}
7570	18.685	18.146	18.882	19.192	-2.280	-1.060	222114	17.906	17.372	18.259	19.317
7262	17.931	17.366	18.233	19.120	-0.400	-4.370	205388	18.200	...	18.286	19.170
7613	17.581	16.769	18.026	19.128	-4.620	-0.680	436170	18.280	18.095	18.526	19.039
6832	18.509	18.104	18.749	19.372	-4.340	-4.520	4758266	18.273	...	18.441	19.381
7339	18.072	17.794	18.418	19.286	6.820	-1.180	4754921	17.913	17.374	18.073	19.059
6837	18.434	17.881	18.697	19.204	-5.230	-5.010	4493242	18.368	17.963	18.575	19.336
6910	18.509	18.166	18.767	19.271	7.920	-0.390	2075930	18.141	17.665	18.310	19.201
7879	18.318	17.934	18.547	19.103	4.330	-8.280	4834944	17.955	...	18.527	19.129
7365	18.475	18.175	18.735	19.168	-2.190	-9.510	754759	18.191	17.891	18.397	19.023
6977	17.813	17.113	18.141	19.278	-7.900	-5.990	3538014	18.310	...	18.683	19.366
47941	18.225	...	18.410	19.340	8.760	4.970	2010372	18.235	17.769	18.420	19.239
8009	17.866	17.602	18.225	19.059	5.340	-8.590	458515	18.204	17.762	18.351	19.352
6902	18.027	17.477	18.458	19.248	-2.350	9.900	207975	18.270	17.640	18.593	19.120
5229	18.376	17.880	18.614	19.148	-2.910	11.000	3535178	18.514	17.777	18.660	19.224
7068	18.432	18.148	18.663	19.353	2.000	-11.370	2043845	18.549	...	18.791	19.320
46237	17.860	17.447	18.090	19.198	8.170	8.190	4810668	17.820	17.261	18.096	19.255
47770	18.540	17.699	18.446	19.115	5.560	10.630	301996	18.659	18.234	18.874	19.236
2751	18.213	17.853	18.533	19.289	-2.770	-12.030	4808345	17.970	17.694	18.147	19.061
5081	18.063	17.455	18.369	19.214	4.390	-12.040	4809815	18.589	17.802	18.699	19.133
50082	18.253	19.299	-9.230	9.280	4716089	18.476	...	18.674	19.366
47144	18.450	17.668	18.657	19.181	13.380	1.520	267466	18.546	17.913	18.769	19.399
5681	18.188	17.659	18.444	19.257	3.170	-13.540	456606	17.812	...	18.251	19.025
51933	18.347	19.254	-11.810	7.990	107259	18.456	18.063	18.710	19.113
1292	18.275	17.609	18.566	19.018	-11.680	-8.570	4739087	18.262	17.584	18.433	19.310
7321	18.285	17.999	18.613	19.255	13.520	-6.350	3481037	18.048	17.666	18.257	19.206
4925	18.522	18.057	18.767	19.216	11.040	-10.640	4752333	18.214	17.723	18.433	19.088
51221	18.333	19.097	-14.700	4.550	4516388	17.853	17.242	18.145	19.200
48269	17.614	16.900	17.974	19.081	16.530	0.380	4861334	18.554	19.278
30161	18.600	...	18.743	19.393	-3.600	16.210	4167605	17.949	17.606	18.163	19.008
20025	18.630	19.348	-8.020	14.750	3444789	18.776	...	18.882	19.385
1398	18.017	17.349	18.360	19.283	-7.410	-15.280	3486482	18.245	17.597	18.478	19.365
1284	18.162	17.680	18.400	19.107	-1.040	-17.420	4041451	17.956	18.311	18.144	19.350
47970	18.284	17.545	18.288	19.185	17.530	0.070	3356230	18.186	17.694	18.382	19.262
47973	18.222	17.703	18.326	19.240	17.580	-0.480	4478587	18.208	17.690	18.408	19.370
48037	18.523	...	18.474	19.346	13.170	11.830	4748703	18.380	...	18.363	19.203
3049	18.250	17.633	18.506	19.393	-17.520	-2.680	4093224	18.051	...	18.218	19.149
43559	18.333	...	18.869	19.180	4.150	17.600	18.083				
2910	18.319	18.014	18.594	19.028	3.810	-17.880	18.281				

Tab.3 (*continued*)

N	V	I	U	m_{255}	X	Y	r
33861	18.184	...	18.423	19.288	-2.260	36.600	36.670
45828	18.311	...	18.543	19.376	28.260	24.840	37.625
45007	18.447	...	18.652	19.187	23.660	29.860	38.097
46434	18.695	...	18.841	19.279	39.330	-0.050	39.330
21809	18.064	17.596	18.250	19.156	-40.500	-8.010	41.285
23822	17.897	17.195	18.271	19.368	-28.660	29.830	41.367
22805	18.356	...	18.436	19.260	-43.880	-2.030	43.927
46857	17.838	17.295	18.095	19.100	42.060	13.900	44.297
45472	17.711	17.046	18.051	19.268	44.490	-4.020	44.671
23181	17.917	17.471	18.193	19.031	-45.260	0.750	45.266
35241	18.212	17.743	18.411	19.222	9.500	45.370	46.354
31833	18.447	18.098	18.616	19.366	5.110	48.290	48.560
32122	18.426	...	18.606	19.275	17.710	45.610	48.928
42948	18.494	...	18.570	19.394	45.670	-22.980	51.126
43517	18.220	17.881	18.415	19.366	25.920	46.460	53.201
34564	17.980	17.360	18.295	19.180	-25.850	47.500	54.078
25134	18.219	17.576	18.418	19.261	-50.680	23.010	55.659
44881	18.179	17.750	18.305	19.301	56.040	-28.440	62.844
44584	18.257	...	18.499	19.284	65.090	13.220	66.419
31898	18.183	17.650	18.409	19.325	-13.450	65.380	66.749
32977	18.315	...	18.540	19.272	27.790	62.190	68.117
41199	18.400	...	18.587	19.111	58.860	47.010	75.329
31316	18.476	...	18.723	19.398	-33.530	67.550	75.414
23960	18.565	18.200	18.757	19.209	-73.000	-22.760	76.466
44882	18.006	...	18.278	19.397	92.550	13.970	93.598

Tab.4 The adopted global BSS sample

Tab.4 (continued)

N	id	V	X	Y	r	GYBS	N	BHS	iBPQ	F93V	X	Y
1	HST7821 [†]	18.176	-1.040	0.610	1.206	1208	44	nHST1855 [†]	oi18.133	-7.430	-12.430	14.
2	HST5866 [†]	17.863	-1.750	1.230	2.139	1141	45	nHST1202	oi18.275	-11.680	-8.570	14.
3	HST7570	18.685	-2.280	-1.060	2.514	1082	46	nHST7321	oi18.285	13.520	-6.350	14.
4	HST5906 [†]	17.510	-2.680	-0.190	2.687	1060	47	41HST48425 [†]	oi18.294	9.640	11.420	14.
5	HST7785 [†]	17.963	-1.110	-2.690	2.910	1196	48	nHST4925	oi18.522	11.040	-10.640	15.
6	HST6674 [†]	16.593	2.210	2.740	3.520	no	49	nHST51221	out ...	-14.700	4.550	15.
7	HST7262	17.931	-0.400	-4.370	4.388	1259	50	nHST20075 [†]	oi17.516	-12.860	9.880	16.
8	HST7613	17.581	-4.620	-0.680	4.670	no	51	nHST45876 [†]	oi17.691	15.970	3.520	16.
9	HST6430 [†]	17.310	-1.930	-4.430	4.832	no	52	nHST1244 [†]	oi18.451	-0.120	-16.510	16.
10	HST5981 [†]	18.016	-2.750	-5.260	5.935	no	53	nHST48269	oi17.614	16.530	0.380	16.
11	HST7678 [†]	17.028	-6.060	-0.870	6.122	802	54	230HST30161	oi18.600	-3.600	16.210	16.
12	HST3736 [†]	17.801	6.050	1.060	6.142	no	55	38HST20025	out ...	-8.020	14.750	16.
13	HST6832	18.509	-4.340	-4.520	6.266	no	56	nHST1398	oi18.017	-7.410	-15.280	16.
14	HST7339	18.072	6.820	-1.180	6.921	no	57	nHST3407 [†]	oi17.434	-11.740	-12.370	17.
15	HST6837	18.434	-5.230	-5.010	7.242	no	58	nHST48119 [†]	oi17.657	8.490	15.030	17.
16	HST6318 [†]	18.166	-1.040	7.790	7.859	no	59	290HST292 [†]	oi17.731	-17.310	-1.870	17.
17	HST6910	18.509	7.920	-0.390	7.930	no	60	nHST1284	oi18.162	-1.040	-17.420	17.
18	HST7850 [†]	18.308	-3.810	-7.120	8.075	966	61	nHST47870	oi18.284	17.530	0.070	17.
19	HST6979 [†]	17.557	9.070	-1.470	9.188	2115	62	nHST47073	oi18.222	17.580	-0.480	17.
20	HST7879	18.318	4.330	-8.280	9.344	1659	63	nHST48037	oi18.523	13.170	11.830	17.
21	HST7365	18.475	-2.190	-9.510	9.759	no	64	nHST3049	oi18.250	-17.520	-2.680	17.
22	HST6977	17.813	-7.900	-5.990	9.914	no	65	nHST7608 [†]	oi17.426	11.840	-13.220	17.
23	HST5313 [†]	17.637	9.670	-2.620	10.019	no	66	56HST43559	oi18.333	4.150	17.600	18.
24	HST47941	18.225	8.760	4.970	10.072	no	67	nHST2910	oi18.319	3.810	-17.880	18.
25	HST8009	17.866	5.340	-8.590	10.115	no	68	nHST1441 [†]	oi17.918	-6.750	-17.110	18.
26	HST6902	18.027	-2.350	9.900	10.175	no	69	nHST5191 [†]	oi17.908	-16.200	-9.070	18.
27	HST6352 [†]	17.799	9.720	-4.800	10.841	2167	70	50HST2424	oi17.906	2.380	-18.420	18.
28	HST5229	18.376	-2.910	11.000	11.378	no	71	nHST20538	oi18.200	-12.520	13.730	18.
29	HST7068	18.432	2.000	-11.370	11.545	no	72	nHST4361	oi18.280	10.420	-15.900	19.
30	HST46237	17.860	8.170	8.190	11.568	no	73	nHST47581	oi18.273	5.420	18.310	19.
31	HST7069 [†]	17.284	1.940	-11.490	11.653	1457	74	nHST47531	oi17.913	19.350	3.100	19.
32	HST47770	18.540	5.560	10.630	11.996	no	75	nHST1498 [†]	oi17.918	-8.610	-17.960	19.
33	HST2751	18.213	-2.770	-12.030	12.345	no	76	nHST44938	oi18.368	7.690	18.610	20.
34	HST5081	18.063	4.390	-12.040	12.815	no	77	nHST4032 [†]	oi17.857	15.340	-13.080	20.
35	HST2926 [†]	17.082	-8.150	-9.960	12.870	613	78	34HST47269 [†]	oi18.005	3.760	20.010	20.
36	HST1769 [†]	16.989	-0.940	-12.960	12.994	1202	79	26HST5214 [†]	oi17.867	19.200	-6.880	20.
37	HST50082	...	-9.230	9.280	13.089	no	80	nHST20753	oi18.141	-18.250	9.290	20.
38	HST47750 [†]	17.734	-1.030	13.280	13.320	no	81	2095HST48349	oi17.955	20.640	-0.900	20.
39	HST47144	18.450	13.380	1.520	13.466	no	82	nHST7547	oi18.191	16.140	-13.090	20.
40	HST47934 [†]	18.114	10.070	9.090	13.566	no	83	63HST46285 [†]	oi17.879	18.550	9.900	21.
41	HST2444 [†]	17.655	-9.140	-10.120	13.636	557	84	nHST35380	oi18.310	-10.200	18.400	21.
42	HST5681	18.188	3.170	-13.540	13.906	no	85	nHST20153	oi18.235	-21.070	-0.170	21.
43	HST51933	...	-11.810	7.990	14.259	no	no	out	out			

Tab.4 (continued)

Tab.4 (continued)

N	id	V	X	Y	r	GYBSN	BHS	iBPQ	F93V	X	Y	
86	HST21131 [†]	17.908	-17.040	13.700	21.864	out 128	nHST23174 [†]	17.934	-30.510	18.460	35.	
87	HST45855	18.204	19.420	10.660	22.153	out 129	nHST47002 [†]	17.045	36.470	2.750	36.	
88	HST2979	18.270	-3.670	-22.590	22.886	out 130	nHST33861	18.184	-2.260	36.600	36.	
89	HST35187 [†]	17.668	-8.090	21.600	23.065	out 131	nHST45828	18.311	28.260	24.840	37.	
90	HST35354	18.514	-4.160	22.770	23.147	out 132	nHST45007	18.447	23.660	29.860	38.	
91	HST21018 [†]	18.014	-22.850	5.490	23.500	out 133	nHST23518 [†]	18.195	-31.800	21.410	38.	
92	HST20438	18.549	-24.150	-1.300	24.185	out 134	nHST45619 [†]	17.305	26.630	27.660	38.	
93	HST47081 [†]	17.998	8.760	23.160	24.761	out 135	nHST46484	18.695	39.330	-0.050	39.	
94	HST48100	17.820	5.780	24.150	24.832	out 136	nF93-32 [†] out	18.226	-29.000	-28.100	40.	
95	HST3019	18.659	-19.130	-16.050	24.971	out 137	nHST21809	18.064	-40.500	-8.010	41.	
96	HST48085	17.970	24.840	2.980	25.018	out 138	nBHS3286 [†]	17.624	-20.810	-35.700	41.	
97	HST48099	18.589	5.620	24.480	25.117	out 139	nHST23862	17.897	-28.660	29.830	41.	
98	HST3189 [†]	17.887	-11.070	-23.040	25.561	out 140	nF93-34 [†] out	18.175	31.800	-26.900	41.	
99	HST47164	18.476	23.510	11.410	26.133	out 141	nF93-36 [†] out	17.818	-3.600	-42.600	42.	
100	HST2070	18.546	-4.520	-25.900	26.291	out 142	nHST23211 [†]	17.078	-43.830	2.730	43.	
101	HST45066	17.812	18.520	19.000	26.533	out 143	nHST22805	18.356	-43.880	-2.030	43.	
102	HST1076	18.456	-22.970	-13.440	26.613	out 144	nHST46857	17.838	42.060	13.900	44.	
103	HST1534 [†]	17.398	0.470	-27.420	27.424	out 145	nHST45472	17.711	44.490	-4.020	44.	
104	HST47590	18.262	19.550	19.270	27.451	out 146	nHST23181	17.917	-45.260	0.750	45.	
105	F93-16 [†]	17.833	-16.300	-22.400	27.703	121 147	nHST23745 [†]	17.838	-44.550	8.730	45.	
106	HST35335 [†]	17.864	-1.940	27.760	27.828	out 148	nHST44630 [†]	18.461	40.320	-21.150	45.	
107	HST34816	18.048	-8.470	26.700	28.011	out 149	nHST34704 [†]	17.675	13.930	43.360	45.	
108	HST47529	18.214	23.260	16.730	28.652	out 150	nHST35241	18.212	9.500	45.370	46.	
109	HST45165	17.853	25.820	12.810	28.823	out 151	nF93-38 [†] out	18.235	38.200	-27.300	46.	
110	HST48012	...	11.080	27.160	29.333	out 152	nHST31883	18.447	5.110	48.290	48.	
111	HST41178	17.949	27.300	10.890	29.392	out 153	nF93-39 [†] out	18.220	1.500	-48.800	48.	
112	HST48164 [†]	17.437	28.250	9.000	29.649	out 154	nHST32112	18.426	17.710	45.610	48.	
113	HST34446	18.776	-16.930	24.630	29.887	out 155	nHST31956 [†]	17.443	7.940	48.910	49.	
114	HST34864	18.245	-0.330	30.150	30.152	out 156	nHST24768 [†]	18.628	-38.720	30.970	49.	
115	HST46418	17.956	30.290	-0.290	30.291	out 157	nHST42948	18.494	45.670	-22.980	51.	
116	HST30784 [†]	18.167	-3.720	30.190	30.418	out 158	nHST43817	18.220	25.920	46.460	53.	
117	HST21270 [†]	17.516	-30.470	-1.410	30.503	out 159	nHST34564	17.980	-25.850	47.500	54.	
118	HST33562	18.186	-16.480	26.930	31.572	out 160	nHST34147 [†]	18.107	3.410	54.180	54.	
119	HST44185	18.208	32.150	5.060	32.546	out 161	nHST25184	18.219	-50.680	23.010	55.	
120	HST47470 [†]	17.609	32.350	-8.320	33.403	out 162	nHST32140 [†]	17.340	2.950	58.400	58.	
121	F93-24 [†]	17.043	-15.300	-30.000	33.676	out 163	nHST20674 [†]	17.843	-50.870	-31.580	59.	
122	HST35310 [†]	18.283	6.870	33.190	33.894	out 164	nHST25414 [†]	18.326	-55.240	24.130	60.	
123	HST47485	18.380	16.460	29.680	33.939	out 165	nF93-45 [†] out	17.222	-10.700	-59.400	60.	
124	HST46932	18.051	11.710	31.870	33.953	out 166	nHST24688 [†]	18.202	-60.880	2.860	60.	
125	HST33784 [†]	17.555	-5.540	33.750	34.202	out 167	nF93-48 [†] out	17.386	5.100	-61.700	61.	
126	HST50012 [†]	...	-30.240	-17.430	34.904	out 168	nHST44881	18.179	56.040	-28.440	62.	
127	F93-26	18.545	26.900	-22.300	34.941	out	no out	26				

Tab.4 (continued)

Tab.4 (continued)

N	id	V	X	Y	r	GYBS	BHSI	BPQ	VF93	X	Y	
169	HST44584	18.257	65.090	13.220	66.419	out 211	F93-83	out 18.572		66.000	-225.000	234
170	HST31898	18.183	-13.450	65.380	66.749	out 212	F93-84	out 18.304		-82.000	222.000	236
171	HST32977	18.315	27.790	62.190	68.117	out 213	F93-85 [†]	out 18.033		37.000	-237.000	239
172	HST21863 [†]	18.075	-61.720	-33.870	70.403	out 214	F93-86 [†]	out 17.950		-205.600	-126.900	241
173	HST23457 [†]	17.870	-68.590	-24.110	72.704	out 215	F93-87	out 18.951		-211.600	116.900	241
174	HST24338 [†]	17.667	-71.860	-16.300	73.685	out 216	F93-88 [†]	out 18.142		33.000	-241.000	243
175	F93-53 [†]	17.609	70.400	-22.500	73.908	out 217	F93-89	out 18.953		61.000	239.000	246
176	HST41199	18.400	58.860	47.010	75.329	out 218	F93-90	out 18.793		226.000	110.000	251
177	HST31316	18.476	-33.530	67.550	75.414	out 219	F93-91	out 18.942		200.000	155.000	253
178	F93-54 [†]	17.476	-62.700	-42.600	75.803	out 220	F93-92	out 18.791		244.000	77.000	255
179	HST26508 [†]	17.824	-63.710	41.630	76.105	out 221	F93-93	out 19.043		-96.000	239.000	257
180	F93-56 [†]	17.467	56.500	-51.200	76.248	out 222	F93-94 [†]	out 17.756		252.000	-63.000	259
181	HST23960	18.565	-73.000	-22.760	76.466	out 223	F93-95	out 18.492		-256.000	51.000	261
182	F93-57 [†]	17.960	34.000	-68.500	76.474	out 224	F93-96	out 18.647		-154.000	-211.000	261
183	HST35060 [†]	16.856	-5.500	76.770	76.967	out 225	F93-97	out 18.710		-263.000	67.000	271
184	HST26142 [†]	17.288	-76.680	14.610	78.059	out 226	F93-98 [†]	out 18.075		55.000	-266.000	271
185	F93-59 [†]	17.678	82.100	-22.600	85.154	out 227	F93-99	out 18.390		-73.000	-262.000	271
186	F93-60 [†]	17.404	86.700	-3.300	86.763	out 228	F93-101	out 18.840		256.000	106.000	277
187	F93-61 [†]	18.218	91.100	-8.400	91.486	out 229	F93-102	out 18.703		70.000	-270.000	278
188	F93-62 [†]	18.173	79.300	-47.100	92.233	out 230	F93-103	out 19.012		279.000	-1.000	279
189	F93-63 [†]	17.061	-9.700	92.700	93.206	out 231	F93-104	out 18.426		257.000	111.000	279
190	HST44882	18.006	92.550	13.970	93.598	out 232	F93-100	out 19.016	no	92.000	-265.000	280
191	F93-64	18.576	90.100	-27.400	94.174	out 233	F93-105	out 18.404	out	-164.000	-235.000	286
192	HST26972 [†]	17.739	-101.480	11.820	102.166	out 234	F93-106 [†]	out 17.722	out	11.000	-287.000	287
193	F93-65 [†]	17.600	-99.000	-33.800	104.611	out 235	F93-107	out 18.633	out	-156.000	-245.000	290
194	F93-66	18.409	90.200	-77.700	119.052	out 236	F93-108 [†]	out 18.200	out	-286.000	52.000	290
195	F93-67 [†]	17.365	99.400	-96.400	138.468	out 237	F93-109	out 18.633	out	104.000	-272.000	291
196	F93-68 [†]	18.112	29.600	167.900	170.489	out 238	F93-110	out 18.390	out	-114.000	278.000	300
197	F93-69 [†]	18.277	-188.500	65.700	199.621	out 239	F93-111 [†]	out 18.146	out	24.000	303.000	303
198	F93-70 [†]	17.477	8.000	-201.000	201.159	out 240	F93-112 [†]	out 18.200	out	-281.000	-118.000	304
199	F93-71	18.891	-176.300	-115.900	210.985	out 241	F93-113 [†]	out 17.913	out	203.000	230.000	306
200	F93-72 [†]	17.418	-185.000	103.500	211.984	out 242	F93-114	out 18.781	out	141.000	273.000	307
201	F93-74 [†]	17.757	-206.500	50.900	212.681	out 243	F93-115 [†]	out 17.524	out	-189.000	244.000	308
202	F93-73	18.724	70.000	201.000	212.840	out 244	F93-116	out 18.408	out	312.000	34.000	313
203	F93-75	18.998	-195.900	88.100	214.799	out 245	F93-117 [†]	out 18.152	out	292.000	124.000	317
204	F93-76	18.723	-207.700	68.300	218.642	out 246	F93-118 [†]	out 17.823	out	-231.000	-225.000	322
205	F93-77	18.732	-191.100	107.600	219.310	out 247	F93-119 [†]	out 17.560	out	283.000	159.000	324
206	F93-78	18.838	62.000	213.000	221.840	out 248	F93-120	out 18.324	out	-285.000	157.000	325
207	F93-79	18.865	-195.600	117.900	228.385	out 249	F93-121	out 18.596	out	233.000	-244.000	337
208	F93-80	18.540	207.000	100.000	229.889	out 250	F93-122	out 18.471	out	-348.000	53.000	352
209	F93-81 [†]	17.611	112.000	202.000	230.972	out 251	S53-124	out 18.317	out	361
210	F93-82 [†]	18.124	65.000	-224.000	233.240	out 252	S53-123 [†]	out 18.477	out	361
						253	S53-125	19.057	out	370

Tab.4 (*continued*)

N	id	V	X	Y	r	GYBS	BHS	BPQ	F93
254	F93-126 [†]	17.791	122.000	351.000	371.598	out	out	out	out
255	F93-127 [†]	17.788	-285.000	-240.000	372.592	out	out	out	out
256	F93-128 [†]	17.380	156.000	350.000	383.192	out	out	out	out
257	S53-129	18.707	410.000	out	out	out	out
258	S53-130	18.717	410.000	out	out	out	out
259	F93-131 [†]	17.506	408.000	-52.000	411.300	out	out	out	out
260	S53-132	18.417	420.000	out	out	out	out
261	S53-133 [†]	18.057	450.000	out	out	out	out
262	S53-134 [†]	18.117	460.000	out	out	out	out
263	S53-135 [†]	17.507	550.000	out	out	out	out

This article was processed by the author using Springer-Verlag
L^AT_EX A&A style file *L-AA* version 3.

This figure "fig2.jpg" is available in "jpg" format from:

<http://arxiv.org/ps/astro-ph/9703026v1>

This figure "fig3.jpg" is available in "jpg" format from:

<http://arxiv.org/ps/astro-ph/9703026v1>

This figure "fig4.jpg" is available in "jpg" format from:

<http://arxiv.org/ps/astro-ph/9703026v1>